ACS Photonics

Article

pubs.acs.org/journal/apchd5

Dynamics of Charge Generation and Transport in Polymer-Fullerene Blends Elucidated Using a PhotoFET Architecture

Ajay K. Pandey,* Muhsen Aljada, Almantas Pivrikas, Marappan Velusamy, Paul L. Burn,* Paul Meredith,* and Ebinazar B. Namdas

Centre for Organic Photonics & Electronics, School of Mathematics and Physics and School of Chemistry and Molecular Biosciences, University of Queensland, Brisbane, Queensland 4072, Australia

Supporting Information

ABSTRACT: High efficiency polymer-fullerene bulk heterojunction organic solar cells can generate photocurrent by excitation of the electron donor and acceptor components via Channel I and Channel II processes, respectively. Using a planar Photo-Field-Effect-Transistor (PhotoFET) architecture operated in steady state and quasi-transient modes we have studied the dynamics of charge generation and transport in blends of PCDTBT/70-PCBM (poly[*N*-9′-heptadecanyl-2,7-carbazole-*alt*-5,5-{4′,7′-di-2-thienyl-2′,1′,3′-benzothiadiazole}]/[6,6]-phenyl-C_{71}-butyric acid methylester). The PhotoFET architecture allows independent measurement of the electron and hole photocurrents and mobilities for charge carriers generated by the Channel I (electron transfer) and Channel II (hole transfer) processes as a function of fullerene content. We find dramatic increases in the photocurrent yield and electron mobility with higher 70-PCBM loading. By analyzing the External Quantum Efficiency (EQE) in *n*- and *p*-PhotoFET modes, we estimate that 80−90% of the photocurrent generated in the optimum 1:4 (polymer/fullerene) blend is derived from fullerene absorption and hole transfer, that is, Channel II.

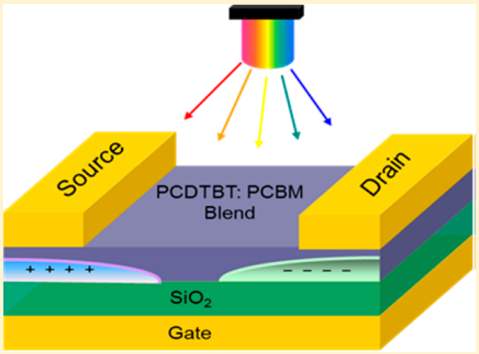

KEYWORDS: *photoFET, polymer solar cells, PCDTBT, channel II photocurrent, quantum efficiency*

Organic solar cells based on solution-processable thin film blends of organic semiconductors are widely viewed as having significant potential in applications such as building integrated and portable solar power.[1,2] The bulk heterojunction (BHJ) architecture to date has been the most successful solution-processed geometry and contains a blend of an electron acceptor and donor as the active junction.[3−6] In this regard, narrow optical gap polymer/fullerene combinations have generated power conversion efficiencies (PCEs) in excess of 9%,[6] with impressive recent progress derived from "materials-based" innovations.[7−10] Understanding the physics of charge generation and extraction (transport) in these new high efficiency systems is a matter of significant scientific interest.[11]

Photocurrent generation in BHJ organic solar cells has been traditionally viewed as arising from light absorption by the donor component followed by photoinduced electron transfer to the acceptor (the so-called Channel I mechanism).[12] However, more recently, it has been appreciated that acceptor absorption can also directly generate significant photocurrent via photoinduced hole transfer to the donor (Channel II).[13−20] This is particularly relevant for some of the narrow optical gap polymers that are reported to be most efficient when used with high loadings of the electron acceptor 70-PCBM ([6,6]-phenyl-C_{71}-butyric acid methylester), which has substantial optical absorption in the solar harvesting window. Hence, it is important to understand how the two photocurrent generation pathways operate and whether they are competitive (whether one is favored over the other), whether they are thermodynamically equivalent, and whether charge generation proceeds via the same charge transfer state intermediate, and once generated, what type of transport pathways are required for efficient extraction.

Light responsive organic field effect transistors (OFETs), or "PhotoFETs", have been used to study the optoelectronic properties of thin film organic semiconductors and devices.[21−29] The focus of these studies and subsequent models have been primarily on the behavior of neat organic semiconductor layers, with very few reports describing photophysical operation of BHJ layers in a PhotoFET architecture.[28−30] Recently, Lombardo and Dodabalapur reported the nongeminate recombination rate in P3HT/60-PCBM (poly[3-*n*-hexylthiophene-2,5-diyl]/([6,6]-phenyl-C_{61}-butyric acid methylester) photovoltaic blends using an OFET geometry.[23] While recognizing that OFET and organic solar cell (OSC) architectures are different, the reported studies indicate that the PhotoFET architecture has the potential to provide important insight into the charge generation and transport physics of OSC materials. In a PhotoFET, charge transport takes place over a few tens of micrometers (i.e., over the channel length), whereas in an organic solar cell this is of

Received: September 20, 2013
Published: January 13, 2014

the order of 100 nm. Generally, as the device length increases, the current density saturates due to the inefficiencies of charge extraction and trapping. In this context it is important to recall that the carrier drift length (λd) is defined by the product of charge carrier mobility, carrier lifetime, and the applied electric field ($\lambda d = \mu\tau E$). If the drift lengths for both electrons and holes are longer than the device lengths (the active layer thickness in a solar cell diode or the channel length in a PhotoFET), then most carriers will exit the active layer without recombination. If this is not the case, then a space charge region will form and recombination will become dominant. Simplistically, and based on this rationale, it is more likely that recombination will limit transport in a PhotoFET channel, which is orders of magnitude greater than the diode thickness. However, an FET is essentially a unipolar device (or at least the conducting channel is), and therefore, photogenerated carriers merely have to traverse a pathway into the channel from the bulk; this makes the organic solar cell diode and PhotoFET almost identical in regard to the carrier diffusion length. Furthermore, the OFET architecture is amenable to both steady-state and transient operation thus enabling information concerning transport dynamics to be probed. In the context of this study it is important to note that exposure of the photosensitive semiconductor layer to light causes changes to the PhotoFET operational parameters. In particular, the PhotoFET operates in two key modes: (i) in the OFF state the PhotoFET shows a photoconductive behavior where hole and electron photocurrent are additive; (ii) in the ON state (particulary at high gate voltages) a photovoltaic behavior is observed where in *n*- (*p*-) mode, photogenerated holes (electrons) produce a shift in the threshold voltage (V_{th}) by (a) changing the occupancy of interface states, (b) acting as counterelectrode, and (c) affecting electron (hole) injection.[28]

In this paper we study a high efficiency polymer/fullerene system, PCDTBT/70-PCBM (poly[*N*-9′-heptadecanyl-2,7-carbazole-*alt*-5,5-{4′,7′-di-2-thienyl-2′,1′,3′-benzothiadiazole}]/[6,6]-phenyl-C_{71}-butyric acid methylester), using the PhotoFET architecture. We investigate the charge generation and transport physics as a function of fullerene loading up to the optimum blend ratio of 1:4. We operate the PhotoFETs in both steady-state and quasi-transient modes under dark, standard white-light, and monochromatic illumination conditions. We are able to independently study both electron and hole currents and carrier mobilities. The measured External Quantum Efficiencies (EQEs) are independent of second order effects such as optical interference, and hence, we are able to compare devices and blends on a "like-for-like" basis and ultimately estimate the photocurrent contributions from both Channels I and II charge generation pathways. These results are particularly valuable in the context of designing balanced, complementary absorber junctions to fully exploit the solar spectral range.

To prepare a PhotoFET, a 350 nm layer of silicon oxide (SiO_2) was grown on a heavily doped Si substrate (University wafer, (100) 0.001−0.005 ohm/cm, SSP, 500 μm prime grade) using an oxidation furnace to form the gate dielectric. The unpolished side of the Si substrate was etched using hydrofluoric acid to remove the SiO_2, followed by sequential deposition of 4 nm of chromium and 50 nm of gold by thermal evaporation to form the gate electrode. The SiO_2 surfaces were coated with hexamethyldisilazane (HMDS), which was spin-coated at 1000 rpm/60 s and dried on a hot plate at 110 °C for 20 min. The PCDTBT/70-PCBM blends were prepared inside a nitrogen filled glovebox at 23 °C with O_2 and H_2O levels <0.1 ppm. The blends were spin-coated onto the treated substrates at 1000 rpm for 60 s and allowed to dry on the hot plate at 70 °C for 20 min resulting in photoactive layer thicknesses in the range of 40−80 nm. Gold top contacts (40 nm) were deposited using a thermal evaporator through shadow masks prepared by deep reactive ion etching with channel lengths (L) 100 μm and channel widths (W) 20 mm.[31] A schematic of the complete PhotoFET architecture is shown in Figure 1 and these devices

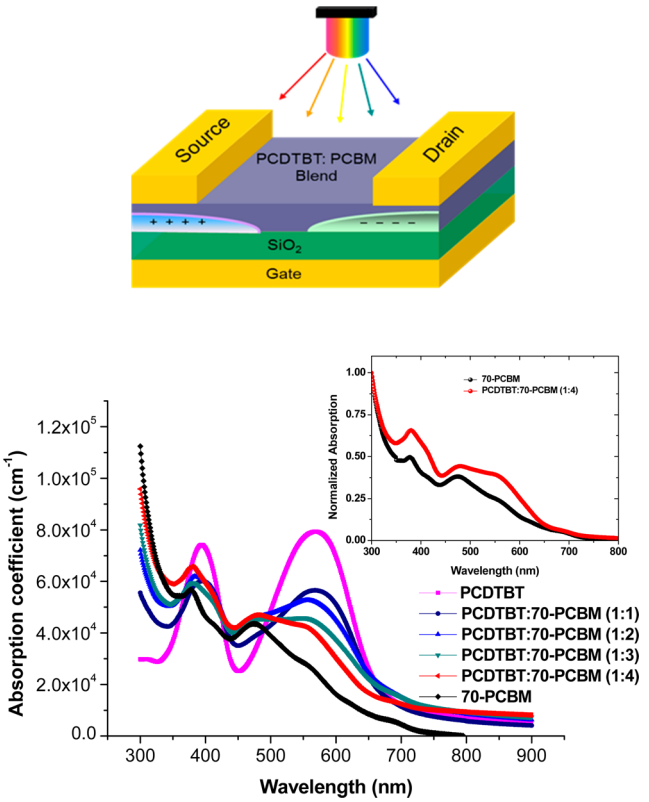

Figure 1. Schematic of a PCDTBT/70-PCBM PhotoFET and the thin film optical absorption spectra of the neat polymer PCDTBT, fullerene 70-PCBM, and polymer/70-PCBM blends at 1:1 to 1:4 (by weight) on glass. The inset compares the absorption profile of the 1:4 blend to that of a neat 70-PCBM thin film on glass.

were characterized using an Agilent B1500A semiconductor parameter characterization system. The gate capacitances of the PhotoFETs were measured using an Agilent Precision Multi-frequency LCR E4980A Meter and found to be 9.2 nF/cm^2. A monochromatic light source, broadband solar simulator (identical to that used to characterize organic solar cells; Abet solar simulator AM1.5, 100 mW/cm^2 standard), and a high intensity pulsed blue LED (Nichia, 470 nm Blue LED) were used for static and quasi-transient photoresponse measurements. It is important to note that >100 devices were fabricated during the course of this study and the static and quasi-transient results presented herein are typical of the average rather than selected for superior performance. The *p*- and *n*-mode EQEs of the PhotoFET devices were obtained using a calibrated silicon photodiode and standard lock-in technique at a chopping frequency of 120 Hz. The mobilities derived from the device transfer characteristics were calculated in the saturation regime using the following formula:

dx.doi.org/10.1021/ph400047b | ACS Photonics 2014, 1, 114−120

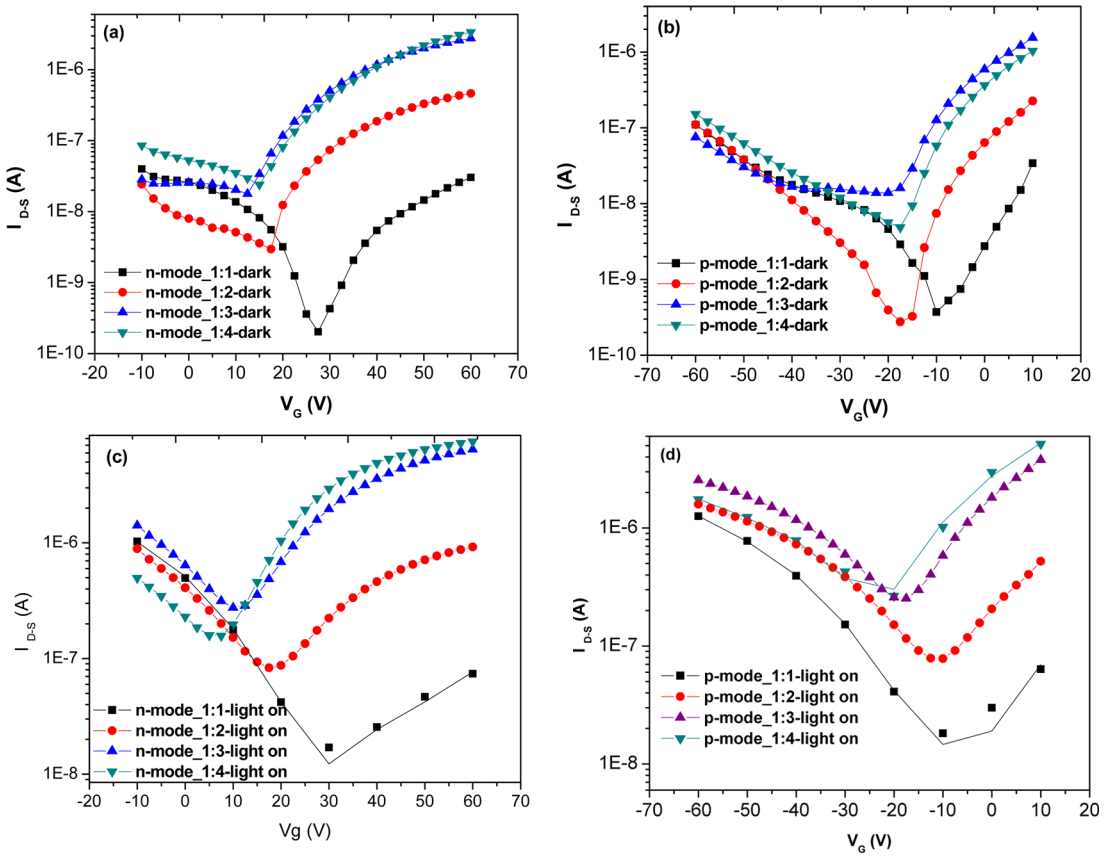

Figure 2. Transfer curves for different blend ratios showing operation of the photoFET ($I_{D\text{-}S}$ vs V_G at V_{DS} = ±30 V) measured in the dark: (a) *n*-mode and (b) *p*-mode, and under illumination from a broad band light source, (c) *n*-mode and (d) *p*-mode. It is evident that, in the dark, the drain current ($I_{D\text{-}S}$) in *n*-mode operation changes significantly as a function of fullerene content, whereas the differences are far less pronounced in the *p*-mode of operation. Under similar measurement conditions, the drain currents ($I_{D\text{-}S}$) under light show significant photoresponse, both in *n*- and *p*-mode.

$$I_d = \frac{W}{2L}\mu \cdot C \cdot (V_g - V_{th})^2 \quad (1)$$

where V_g is the gate voltage, I_d is the source-drain current, V_{th} is the threshold voltage, μ is the channel mobility, C is gate capacitance, W is the channel width, and L is the channel length.

We first investigated the changes in active junction thin film absorption as a function of the PCDTBT/70-PCBM blend ratio (Figure 1). The spectra capture the evolution of blend absorption in 1:1, 1:2, 1:3, and 1:4 ratios as compared to the individual component absorptions of PCDTBT and 70-PCBM. It is important to note that we used a constant polymer concentration (7 mg/mL) and deposition spinning speed (1000 rpm) for all blends and varied the amount of fullerene. Hence, the differences in film thickness are solely due to the increasing amount of 70-PCBM. As expected, the PCDTBT absorption has two peaks, at 390 and 560 nm, with a tail extending into the red, and a region of lower optical absorption centered at ∼450 nm. The absorption spectrum of 70-PCBM is broad and comprised of a series of shoulders, and peaks at 376 and 472 nm, the second of which fits nicely into the region where PCDTBT has low optical absorption. The thicknesses of the two single component films were ∼45 nm, yielding extinction coefficients of order of 7.4×10^4 cm^{-1} (390 nm) and 7.9×10^4 cm^{-1} (560 nm) for PCDTBT and 3.9×10^4 cm^{-1} (450 nm) for 70-PCBM. The absorption spectrum of the 1:1 blend is similar to the optical profile of the neat PCDTBT film. However, blends of 1:2 PCDTBT/70-PCBM and higher show a significant departure from the absorption spectrum of PCDTBT as the fullerene component begins to dominate the spectrum. At a 1:4 PCDTBT/70-PCBM ratio the absorption spectrum is very similar to the neat 70-PCBM film (inset Figure 1). In the context of this work, the peak at 480 nm is a fingerprint that we subsequently use in analyzing the EQE of the blends.

Next, to understand free carrier generation and collection we investigated the spectral photoresponse of the PCDTBT/70-PCBM FETs as a function of blend ratio. It is important to note that the photocurrents measured in either FET or diode devices depends upon several factors, notably, the efficiency of free carrier generation from absorbed photons and the extraction efficiency. It is often very difficult to disentangle these two phenomena. Figure 2a,b shows the transfer curves of PhotoFETs with different blend ratios of PCDTBT/70-PCBM in both *n*- and *p*-modes measured in the dark. An interesting observation is that the current flow ($I_{D\text{-}S}$) in *n*-mode operation (V_{DS} and V_G; +ve) shows a strong correlation with the amount of fullerene present in the blend, whereas the current flow in *p*-mode (V_{DS} and V_G; -ve) shows a much weaker dependence on fullerene content. Under illumination, as detailed in Figure 2c,d, a significant increase in both *n*- and *p*-mode current flow is observed confirming that extra current is being generated following absorption of photons by the fullerene and polymer, respectively. We now turn our attention

dx.doi.org/10.1021/ph400047b | ACS Photonics 2014, 1, 114−120

to whether there is a blend ratio dependence of the charge transport, particularly for electron transport through the fullerene phase. For a detailed comparison of *n*- and *p*- mode operation in the dark and under illumination from a broad-band light source, see Supporting Information, Figures S1−S4.

First, we looked at the current−voltage curves measured in the dark and extracted electron and hole mobilities from the saturation regime (high gate voltage) of PhotoFET operation. The complete evolution of charge transport at different blend ratios is captured in Figure 3a. We observe that in the 1:1 blend

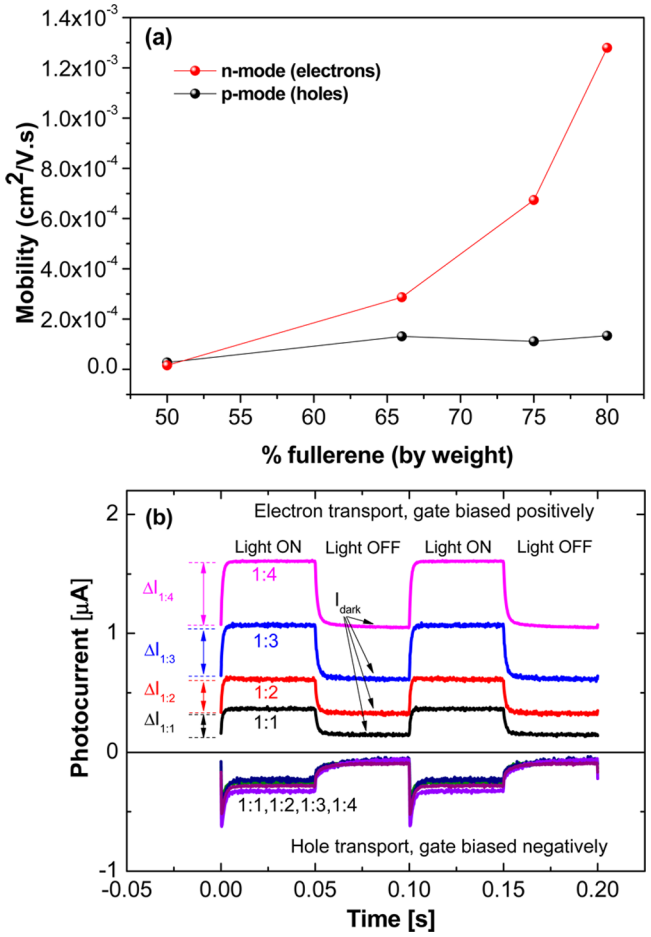

Figure 3. (a) Electron and hole mobilities measured *in the dark* for different blend ratios extracted from FET *I*−*V* (current−voltage) measurements. (b) Quasi-transient dark (operated in the linear regime (V_G = ±60 V, V_{DS} = ±5 V)) and photocurrent responses obtained using a fast (rise time < 10 ns) 470 nm LED. The photocurrent response in each different blend is labeled by $\Delta I_{blend/ratio}$, while the I_{dark} shows the steady state dark injection current. The relative change in photocurrent signals arise due to the differences in the quantum efficiency for mobile charge carrier generation and collection, while the relative changes in steady state dark injection currents are purely due to the difference in charge carrier mobility.

the electron and hole mobilities are both of order 10^{-5} cm^2/(V s). As the fullerene content gets larger, there is an increase in electron mobility, reaching $\mu_e \approx 1 \times 10^{-3}$ cm^2/(V s) for the 1:4 blend ratio. In fact, the μ_e of around 10^{-3} cm^2/(V s) is similar to that reported for neat 70-PCBM films showing that the presence of the polymer does not have a detrimental effect.[32] In contrast, the hole mobility stays relatively constant for the different blends. It should be noted that these results also show that there is blend of the materials at the interface. If the fullerene accumulated at the interface then the measured hole mobility would have decreased with increasing fullerene content. A summary of the dark PhotoFET characteristics is provided in Table S1. Figures S1−S4 also show the source-drain current voltage characteristics under a broadband white light source (Abet solar simulator AM1.5, 100 mW/cm^2 standard). The mobility trends under illumination are the same as those seen in the dark measurements, that is, a large increase in the electron mobility as a function of increased fullerene loading.

In the next part of the study, a fast (rise time < 10 ns) pulsed LED (470 nm emission) was used to study the quasi-transient responses of the PhotoFETs as a function of blend ratio in order to elucidate the relative efficiencies of photocurrent generation. These measurements were also performed in both *n*- and *p*-transistor modes (high positive and negative gate voltages, respectively) to isolate the electron and hole properties. To ensure a homogeneous carrier distribution in the conducting channels of the PhotoFETs, the source-drain voltages were kept low and the devices were operated in the linear regime (V_G = ±60 V, V_{DS} = ±5 V). The use of the linear regime, in some sense, at least partially mimics conditions of volume carrier generation in an operational solar cell. Figure 3b shows the transient photoresponses (*n*- and *p*-) for all blend ratios where I_{dark} represents the dark injection current and $\Delta I_{blend/ratio}$ is the transient photocurrent. The relative changes in photocurrent signals arise due to differences in the quantum efficiency for mobile charge carrier generation and collection (photocurrent yield), while the relative changes in the steady state dark injection currents are purely due to differences in mobility (in full agreement with the dark static measurements). Figure 3b shows a clear increase in $\Delta I_{blend/ratio}$ as a function of higher fullerene loading for the n-channel. For the n-channel, the ratio between the dark current of the different blends is the same as when the light was on. Therefore, the efficiency of free charge generation appears to be the same for each of the blends and the increase in photocurrent yield is due to the increase in electron mobility in moving from the 1:1 to 1:4 polymer/fullerene blends. In contrast, the *p*-mode operation shows different dynamics with a short-lived initial spike appearing on illumination before an equilibrium photocurrent is measured. Unlike the *n*-mode operation, there is not a significant change in the photocurrent (either in the dark or light) with blend ratio, which is consistent with the mobilities shown in Figure 3a. Thus, the static and quasi-transient results indicate that changes to the EQE as a function of blend ratio arise due to differences in the mobility and charge collection.

To further determine the origin of photocurrent improvements as the blend ratio is increased, we also assessed the spectral dependence of the photoresponse via static EQE measurements in *n*- and *p*-transistor modes. While the shape of the EQE in an organic solar cell is dependent upon a number of factors: the quantum efficiency for free carrier generation; the extraction efficiency (free carrier transit time vs lifetime); optical cavity effects; and parasitic absorptions in the non-active heterojunction layers; for these EQE measurements, we can neglect the latter two since the PhotoFET cavity is extremely low finesse and we illuminate through an air-junction (active layer) interface. Figure 4a,b shows the *p*- and *n*-mode monochromatic EQE responses, respectively, recorded at V_G = ±60 V and V_{DS} = ±30 V. They represent, respectively, the photogeneration and extraction of holes and electrons as a

dx.doi.org/10.1021/ph400047b | ACS Photonics 2014, 1, 114−120

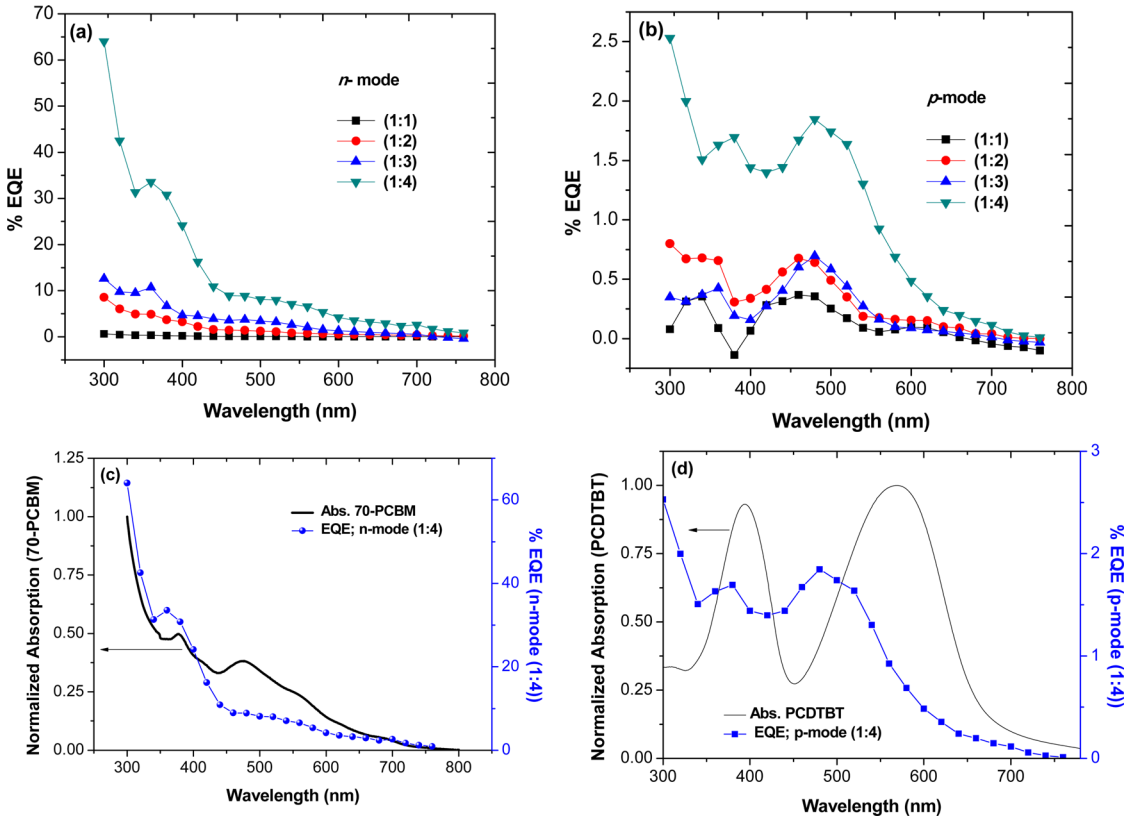

Figure 4. External quantum efficiency (EQE) of the PCDTBT/70-PCBM blends (1:1, 1:2, 1:3, 1:4) obtained with the PhotoFET operating in (a) *n*-mode and (b) *p*-mode recorded at $V_G = \pm 60$ V and $V_{DS} = \pm 30$ V. (c) The EQE of the 1:4 ratio PCDTBT/70-PCBM PhotoFET in *n*-mode and a comparison with the absorption of a neat 70-PCBM film. (d) The EQE of the 1:4 ratio PCDTBT/70-PCBM PhotoFET in *p*-mode and a comparison with the absorption of a neat PCDTBT film.

function of incident light wavelength and blend ratio. The results show that in general, the shapes of the EQE spectra as a function of fullerene loading are essentially the same confirming that optical cavity effects are not first order given the film thickness differences. Looking in detail at the 1:4 blend EQE we see in Figure 4c that the *n*-mode response shows a close spectral correspondence to the 70-PCBM absorption spectrum. In contrast, the *p*-mode EQE bears little resemblance to the PCDTBT absorption and in fact also looks more 70-PCBM-like. Furthermore, the *n*-mode EQE has a peak at ∼60%, while the *p*-mode EQE is just 2%. This strongly suggests that a significant fraction of both the electron and hole photocurrents arise from direct absorption by the fullerene component followed by photoinduced hole transfer to the donor component (i.e., Channel II). For completeness, we present the photocurrent measured in *n*- and *p*-mode for all blend ratios in the Supporting Information (Figure S5).

Using this EQE data, we can estimate the fraction of photocurrent generated by light absorption of the fullerene and PCDTBT components (i.e., Channels II and I, respectively) using

$$J = \frac{1}{S}\int_{\lambda=\min}^{\lambda=\max} \varphi(\lambda)\cdot \mathrm{EQE}(\lambda)\mathrm{d}\lambda \qquad (2)$$

where S is the active surface area of the PhotoFET channel, φ is the AM 1.5 solar photon-flux, EQE is the external quantum efficiency of *p*- or *n*-mode operation, and $\lambda_{max/min}$ is the absorption wavelength range of the PCDTBT/70-PCBM blend. The integration of the *n*-mode EQE presented in Figure 4c thus gives a photocurrent density of 1.86 mA/cm^2. A similar calculation on the *p*-mode EQE presented in Figure 4d produces a photocurrent density of 0.21 mA/cm^2. This suggests that fullerene absorption could contribute up to as much as 90% to the total photocurrent in the 1:4 blend ratio. We once again note that, due to architectural differences between our PhotoFETs and normal cell diode geometries, the actual percentage of photocurrent contribution could be different in operational solar cell devices, but clearly, the 70-PCBM component appears to be the dominant partner at blend ratios optimized for the highest conversion efficiencies.

In conclusion, we have shown that a planar PhotoFET architecture can provide important information with regard to the origin of photocurrent generation as a function of fullerene loading in model bulk heterojunction layers. In particular for the high efficiency organic solar cell blend PCDTBT/70-PCBM static dark $I-V$ measurements show an increase in electron mobility as the 70-PCBM fraction approaches the optimum 1:4 blend ratio, while the hole mobility remains relatively constant. These findings are confirmed by monochromatic quasi-transient measurements where we also see *n*-type mobility enhancement. Steady-state monochromatic EQE results obtained in both *n*- and *p*-transistor modes further confirm these findings and indicate that Channel II is the dominant operational photocurrent generation pathway in the optimized blends. Integration of the EQE spectra for the 1:4 system would suggest that as much as 90% of the photocurrent is produced by light absorption in the fullerene followed by photoinduced hole transfer to the polymer. Although the planar PhotoFET architecture differs in several key aspects from an operational

dx.doi.org/10.1021/ph400047b | *ACS Photonics* 2014, 1, 114−120

organic solar cell, the ability to isolate electron and hole currents has great potential for studying organic semiconductor blends.

■ ASSOCIATED CONTENT

Supporting Information

A table showing PhotoFET operational parameters (Table S1), additional figures (Figures S1−S4) showing full output characteristics of the PhotoFETs (for all blend ratios; measured in dark and under illumination), and spectral photoresponse of PhotoFETs operated in *n*- and *p*-mode (Figure S5) are presented. This material is available free of charge via the Internet at http://pubs.acs.org.

■ AUTHOR INFORMATION

Corresponding Author

*E-mail: a.pandey@uq.edu.au; p.burn2@uq.edu.au; meredith@physics.uq.edu.au.

Notes

The authors declare no competing financial interest.

■ ACKNOWLEDGMENTS

P.M. and P.L.B. are Vice Chancellor's Senior Research Fellows, A.K.P. is the recipient of an Australian Renewable Energy Agency (ARENA) Research Fellowship (Project 6-F022), A.P. is the recipient of an Australian Research Council (ARC) Discovery Early Career Researcher Award, and E.B.N. is an ARC Future Fellowship Award holder. We acknowledge funding from the University of Queensland (Strategic Initiative − Centre for Organic Photonics & Electronics) and the Australian Solar Institute ("Organic Solar Cells Beyond the Shockley-Queisser Limit"). This work was performed in part at the Queensland node of the Australian National Fabrication Facility (ANFF), a company established under the National Collaborative Research Infrastructure Strategy to provide nano and microfabrication facilities for Australia's researchers.

■ REFERENCES

(1) Li, G.; Zhu, R.; Yang, Y. Polymer solar cells. *Nat. Photonics* **2012**, *6*, 153−161.

(2) Graetzel, M.; Janssen, R. A. J.; Mitzi, D. B.; Sargent, E. H. Materials interface engineering for solution-processed photovoltaics. *Nature* **2012**, *488*, 304−312.

(3) Yu, G.; Gao, J.; Hummelen, J. C.; Wudl, F.; Heeger, A. J. Polymer photovoltaic cells: enhanced efficiencies via a network of internal donor-acceptor heterojunctions. *Science* **1995**, *270*, 1789−1791.

(4) Park, S. H.; Roy, A.; Beaupré, S.; Cho, S. S.; Coates, N.; Moon, J. S.; Moses, D.; Leclerc, M.; Lee, K.; Heeger, A. J. Bulk heterojunction solar cells with internal quantum efficiency approaching 100%. *Nat. Photonics* **2009**, *3*, 297−302.

(5) Pandey, A. K.; Aljada, M.; Velusamy, M.; Burn, P. L.; Meredith, P. Nanostructured, active organic−metal junctions for highly efficient charge generation and extraction in polymer-fullerene solar cells. *Adv. Mater.* **2012**, *24*, 1055−1061.

(6) He, Z.; Zhong, C.; Su, S.; Xu, M.; Wu, H.; Cao, Y. Enhanced power-conversion efficiency in polymer solar cells using an inverted device structure. *Nat. Photonics* **2012**, *6*, 591−595.

(7) Coffin, R. C.; Peet, J.; Rogers, J.; Bazan, G. C. Streamlined microwave-assisted preparation of narrow-bandgap conjugated polymers for high-performance bulk heterojunction solar cells. *Nat. Chem.* **2009**, *1*, 657−661.

(8) Liang, Y. Y.; Yu, L. P. A new class of semiconducting polymers for bulk heterojunction solar cells with exceptionally high performance. *Acc. Chem. Res.* **2010**, *43*, 1227−1236.

(9) Zhou, H. X.; Yang, L. Q.; Liu, S. B.; You, W. A tale of current and voltage: interplay of band gap and energy levels of conjugated polymers in bulk heterojunction solar cells. *Macromolecules* **2010**, *43*, 10390−10396.

(10) Boudreault, P. L. T.; Najari, A.; Leclerc, M. Processable low-bandgap polymers for photovoltaic applications. *Chem. Mater.* **2011**, *23*, 456−469.

(11) Deibel, C. Photocurrent generation in organic solar cells. *Semicond. Semimetals* **2011**, *85*, 297−330.

(12) Sariciftci, N. S.; Smilowitz, L.; Heeger, A. J.; Wudl, F. Photoinduced electron transfer from a conducting polymer to buckminsterfullerene. *Science* **1992**, *258*, 1474−1476.

(13) Wienk, M. M.; Kroon, J. M.; Verhees, W. J. H.; Knol, J.; Hummelen, J. C.; van Hal, P. A.; Janssen, R. A. J. Efficient methano[70]fullerene/MDMO-PPV bulk heterojunction photovoltaic cells. *Angew Chem., Int. Ed.* **2003**, *42*, 3371−3375.

(14) Dastoor, P. C.; McNeill, C. R.; Frohne, H.; Foster, C. J.; Dean, B.; Fell, C. J.; Belcher, W. J.; Campbell, W. M.; Officer, D. L.; Blake, I. M.; Thordarson, P.; Crossley, M. J.; Hush, N. S.; Reimers, J. F. Understanding and improving solid-state polymer/C60-fullerene bulk-heterojunction solar cells using ternary porphyrin blends. *J. Phys. Chem. C* **2007**, *111*, 15415−15426.

(15) Yao, Y.; Shi, C. J.; Li, G.; Shrotriya, V.; Pei, Q. B.; Yang, Y. Effects of C70 derivative in low band gap polymer photovoltaic devices: Spectral complementation and morphology optimization. *Appl. Phys. Lett.* **2006**, *89*, 153507.

(16) Burkhard, G. F.; Hoke, E. T.; Scully, S. R.; McGehee, M. D. Incomplete exciton harvesting from fullerenes in bulk heterojunction solar cells. *Nano Lett.* **2009**, *9*, 4037−4041.

(17) Nicolaidis, N. C.; Routley, B. S.; Holdsworth, J. L.; Belcher, W. J.; Zhou, X. J.; Dastoor, P. C. Fullerene contribution to photocurrent generation in organic photovoltaic cells. *J. Phys. Chem. C* **2011**, *115*, 7801−7805.

(18) Koster, L. J. A.; Shaheen, S. E.; Hummelen, J. C. Pathways to a new efficiency regime for organic solar cells. *Adv. Energy Mater.* **2012**, *2*, 1246−1253.

(19) Fang, Y.; Pandey, A. K.; Nardes, A. M.; Kopidakis, N.; Burn, P. L.; Meredith, P. A narrow optical gap small molecule acceptor for organic solar cells. *Adv. Energy Mater.* **2013**, *3*, 54−59.

(20) Zhang, M.; Pandey, A. K.; Tandy, K.; Dutta, G. K.; Burn, P. L.; Meredith, P.; Namdas, E. N.; Patil, S. Channel II photocurrent quantification in narrow optical gap polymer-fullerene solar cells with complimentary acceptor absorption. *Appl. Phys. Lett.* **2013**, *102*, 223302.

(21) Narayan, K. S.; Kumar, N. Light responsive polymer field-effect transistor. *Appl. Phys. Lett.* **2001**, *79*, 1891−1893.

(22) Singh, T. B.; Koeppe, R.; Sariciftci, N. S.; Morana, M.; Brabec, C. J. Monitoring the channel formation in organic field-effect transistors via photoinduced charge transfer. *Adv. Funct. Mater.* **2009**, *19*, 789−795.

(23) Lombardo, C.; Dodabalapur, A. Nongeminate carrier recombination rates in organic solar cells. *Appl. Phys. Lett.* **2010**, *97*, 233303.

(24) Noh, Y.-Y.; Kim, D.-Y.; Yase, K. Highly sensitive thin-film organic phototransistors: Effect of wavelength of light source on device performance. *J. Appl. Phys.* **2005**, *98*, 074505.

(25) Rao, M.; Ortiz, R. P.; Fachetti, A.; Marks, T. J.; Narayan, K. S. Studies of photogenerated charge carriers from donor-acceptor interfaces in organic field-effect transistors: implications for organic solar cells. *J. Phys. Chem. C* **2010**, *114*, 20609−20613.

(26) Cho, S.; Yuen, J.; Kim, J. Y.; Lee, K.; Heeger, A. J. Photovoltaic effects on the organic ambipolar field-effect transistors. *Appl. Phys. Lett.* **2007**, *90*, 063511.

(27) Wasapinyokul, K.; Milne, W. I.; Chu, D. P. Photoresponse and saturation behavior of organic thin film transistors. *J. Appl. Phys.* **2009**, *105*, 024509.

(28) Wang, X.; Wasapinylokul, K.; Rawcliffe, R.; Campbell, A. J.; Bradely, D. D. C. Device physics of highly sensitive thin film polyfluorene copolymer organic phototransistors. *J. Appl. Phys.* **2010**, *107*, 024509.

(29) Baeg, K.-J.; Binda, M.; Natali, D.; Caironi, M.; Noh, Y.-Y. Organic light detectors: photodiodes and phototransistors. *Adv. Mater.* **2013**, *31*, 4267−4295.
(30) Ng, T. N.; Fujieda, I.; Street, R. A.; Veres, J. Persistent photoconductivity effects in printed n-channel organic transistors. *J. Appl. Phys.* **2013**, *113*, 094506.
(31) Aljada, M.; Mutkins, K.; Vamvounis, G.; Burn, P. L.; Meredith, P. High quality shadow masks for top contact organic field effect transistors using deep reactive ion etching. *J. Micromech. Microeng.* **2010**, *20*, 075037.
(32) Anthopoulos, T. D.; de Leeuw, D. M.; Cantatore, E.; van 't Hof, P.; Alma, J.; Hummelen, J. C. Solution processible organic transistors and circuits based on a C70 methanofullerene. *J. Appl. Phys.* **2005**, *98*, 054503.